Supporting Information for Publication

In-Situ Electrochemical Transformation of Ni^{2+} to NiOOH as an Effective Electrode for Water Oxidation Reaction

Sangeetha Kumaravel,[†‡] Rishivandhiga Jayakumar,[†] Karthik Kumaran Saravanan,[†] Vennala Niharika,[†] Bariki Eunice Evangeline,[†] Vengatesan Singaram[†‡] and Subrata Kundu[†‡*]

[†]*Electrochemical Process Engineering (EPE) Division, CSIR-Central Electrochemical Research Institute (CECRI), Karaikudi-630003, Tamil Nadu, India.*

[‡] *Academy of Scientific and Innovative Research (AcSIR), Ghaziabad-201002, India.*

*To whom correspondence should be addressed, *E-mail:* *skundu@cecri.res.in* *and* *kundu.subrata@gmail.com*, Tel: +91 4565-241487.

This file contains pages from S1 to S30, where the detailed, reagents and instruments used in the study, figures and Tables corresponding to NiOOH@GDL has been given.

Number of Pages: 30

Number of Figures: 17

Number of Tables: 03

Reagents and Instrumental details

The precursor, Nickel (II) acetate tetrahydrate ($Ni(OCOCH_3)_2.4H_2O$), Potassium Hydroxide (KOH) were procured from Sigma Aldrich. Hg/HgO (reference electrodes) was purchased from the Aut-M204 auto-lab instrument and the carbon cloth (GDL) (counter electrode) were purchased from Alfa- Aesar. The entire OER study was carried out using Auto lab-M204 instrument purchase from Metrohm Pvt Ltd, Netherlands. Deionized water (DI) was used for the synthesis of different concentration NiOOH@GDL catalyst and its characterization. The NiOOH@GDL electrocatalyst was characterized using various techniques such as XRD, XPS, Raman, FE-SEM, HR-TEM, EDS and HADDF analysis.

The X-ray diffraction (XRD) analysis was carried out using a X-RAY Diffractometer D8 Advance, Bruker with Cu Kα radiation (λ = 0.154178 nm) with a scanning rate of 5° min^{-1} in the 2θ range 10-80°, with a power of 40 KV; 30 mA. The X-ray photoelectron spectroscopic (XPS) analysis was done to study the oxidation state of elements present in the materials and analysed by using ESCALAB 250xi Base System XR6 Micro-focused Monochromator (Al Kα XPS) XR4 Twin Anode Mg/Al (300/400W) X-Ray Source, EX06 Ion gun. The LASER Raman measurements were carried out with LabRAM HR Evolution, Horiba Jobin Yvon Raman Microscope using an excitation wavelength of 532 nm (He-Ne laser). The structural studies and the High-angle annular dark-field imaging (HAADF) colour mapping of both the electrocatalyst was carried in HR-TEM, (FEI, Netherland, Talos F200S) working at an accelerating voltage of 200 kV. The Energy Dispersive X-ray Spectroscopy (EDAX) analysis was done with the HR-TEM instrument with a separate EDAX detector (SDD) connection. Further, the Field Emission Scanning Electron Microscope (FE-SEM) analysis was performed using SUPRA 55VP, Gemini Column with air lock system (Carl Zeiss, Germany). The X-ray fluorescence (XRF) analysis was carried out using XGT-5200 (Horiba, Japan) X-ray analytical microscope with X-ray tube 50 kV.

Ink preparation method for fabricating commercial NiO electrocatalyst over CC

For comparison, the commercially available NiO was procured. Then 3 mg of the NiO catalyst was taken in the solution containing 750 μL DI H_2O, 250 μL ethanol and 50 μL of nafion and the solution was kept at sonication for 30 minutes, the well-dispersed brown colour solution was appeared. From there, 34.5 μL of solution was drop-casted to the carbon cloth (CC) over the area of (1 × 0.5 cm^2). Before drop-casting, the bare CC was dipped in the DI water and solicited for 15 minutes and turned to hydrophilic in nature. Further, the coated

NiO was kept at drying for complete night in the hot oven at 50 °C. Finally, the mass loading calculated for the commercial NiO was 0.205 mg cm^{-2} and the same has been proceed for the electrochemical studies.

Calculating ECSA from the redox features of CV

The integrated area of the redox peak of Ni^{2+} to Ni^{3+} = 0.00227 VA

The associated energy at the corresponding potential = 0.00227 VA / 0.005 Vs^{-1}

$$Q = I \times t$$

$$I = Q/t$$

$$\text{Charge, } Q = 0.454 \text{ AS}$$

Now, the number of electron transferred is = 0.454 C / 1.602×10^{-19} C

$$= 0.283 \times 10^{19}$$

Since, the reduction of Ni^{3+} to Ni^{2+} is a single electron transfer process, the number electron calculated above is exactly the same as the number of surface active sites.

Hence,

The number of Ni that participated in OER is = 2.83×10^{18} for NiOOH@GDL-A

Similarly, we have calculated the ECSA value from the integrated area of the redox peak and given in the below table.

Catalysts	Integrated area (VA) from the redox CV curve	ECSA value from redox curve
NiOOH@GDL-A	0.00227	2.83×10^{18}
NiOOH@GDL-B	0.00801	1.0×10^{19}
NiOOH@GDL-C	0.00268	3.34×10^{18}

Turn over Frequency calculation

The TOF was calculated using the following formula,

$$\mathbf{TOF = j \times N_A / F \times n \times \Gamma}$$

Here, **j** is the current density in A cm^{-2}, $\mathbf{N_A}$ is the geometrical surface area, **F** is the Faradaic constant (96 485 C mol^{-1}), **n** is the number of electron involved during OER, **Γ** is the surface concentration calculated from the ECSA during redox curve.

Using the above equation, the TOF was calculated for all the four catalyst such as NiOOH@GDL-A, NiOOH@GDL-B and NiOOH@GDL-C.

NiOOH@GDL-A = $(9.97 \times 10^{-3}) \times (6.023 \times 10^{23}) / (2.83 \times 10^{18})\,(4)\,(96485)$

NiOOH@GDL-A = $5.497 \times 10^{-7}\ S^{-1}$

NiOOH@GDL-A = $(22.66 \times 10^{-3}) \times (6.023 \times 10^{23}) / (1 \times 10^{19})\,(4)\,(96485)$

NiOOH@GDL-A = $35.321 \times 10^{-7}\ S^{-1}$

NiOOH@GDL-A = $(18.80 \times 10^{-3}) \times (6.023 \times 10^{23}) / (3.34 \times 10^{18})\,(4)\,(96485)$

NiOOH@GDL-A = $8.784 \times 10^{-7}\ S^{-1}$

Mass activity calculation

Current observed in particular potential for the NiOOH@GDL-B and Comm. NiO

Mass loading calculated for NiOOH@GDL-B = 0.607 mg cm^{-2}

Comm. NiO = 0.205 mg cm^{-2}

Fixed Overpotential (V)	Current density of NiO in mA cm^{-2}	Current density of NiOOH@GDL-A in mA cm^{-2}
1.5	0.551	11.582
1.55	0.339	35.101
1.6	3.211	62.451

Mass activity is calculated using the formulae,

Mass activity = Current density/Loading of a catalyst

Hence,

Mass activity calculated = 3.211/0.205 = 15.669 mg cm^{-2} for NiO at 1.6 V

Mass activity calculated = 62.451/0.607 = 102.886 mg cm^{-2} for NiOOH@GDL-A at 1.6 V

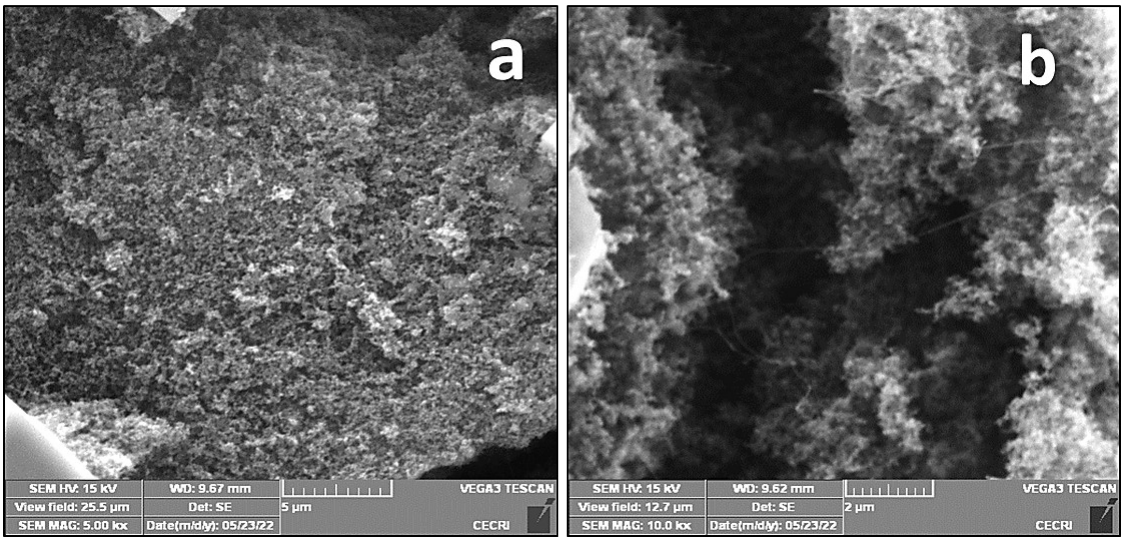

Figure S1. (a and b) SEM images of GDL surface after 10 cycling of NiOOH @GDL-A and NiOOH @GDL-C catalysts.

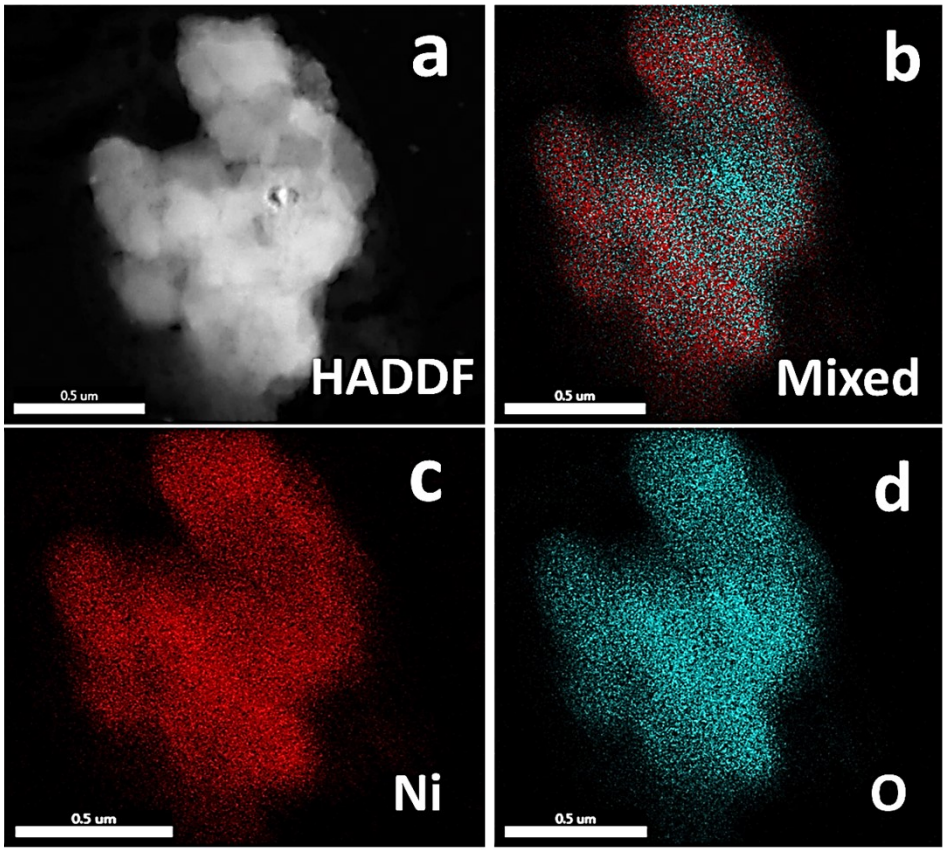

Figure S2. (a) High-angle annular dark-field imaging (HAADF**)** image of NiOOH@GDL-B; (b) overlapped elemental mapping of Ni and O and (c and d) individual colour mapping of Ni and O.

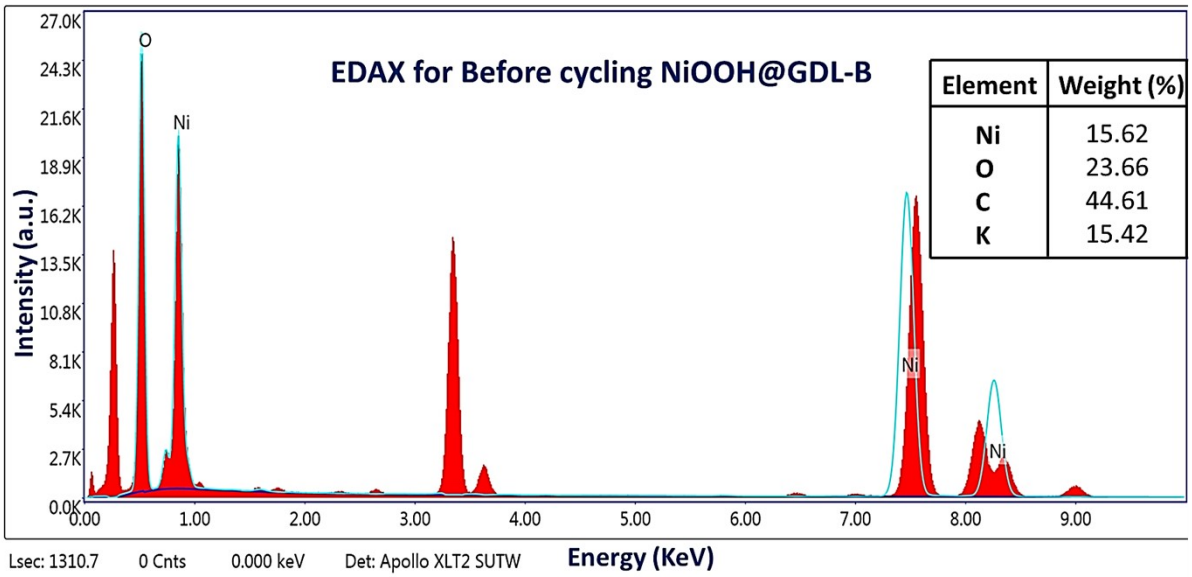

Figure S3. EDAX spectra of before cycling NiOOH@GDL-B shows the elemental presence of Ni, O, C and K.

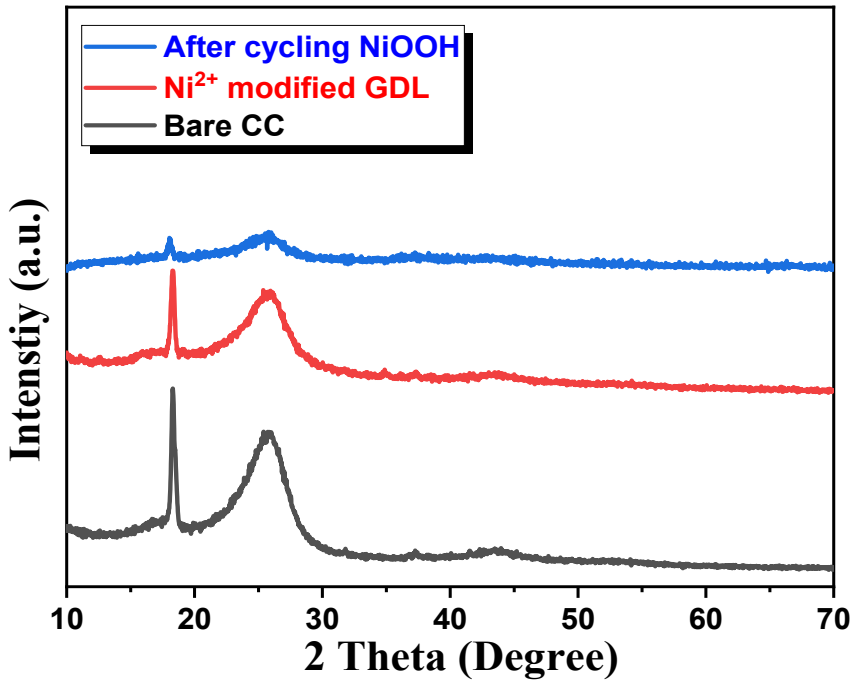

Figure S4. Stacked XRD pattern for Bare CC, Ni^{2+} modified GDL and after cycling NiOOH.

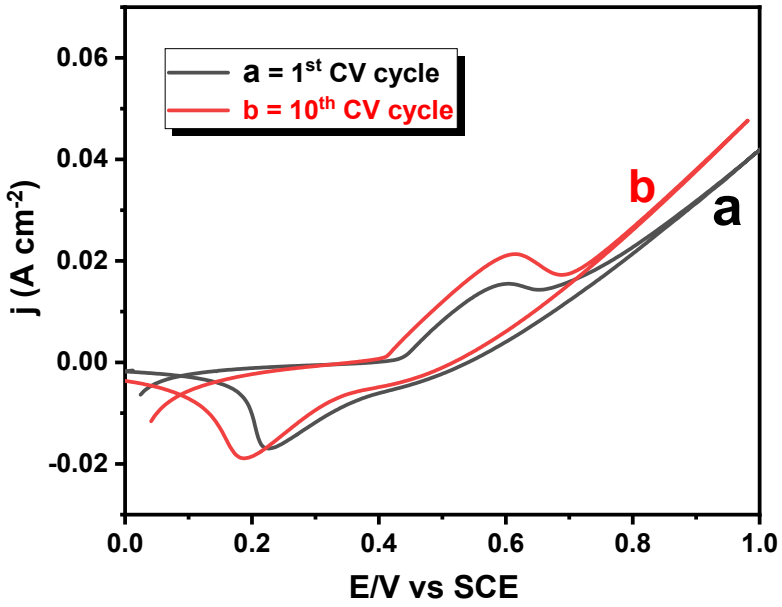

Figure S5. CV curve during first and tenth cycle of activation step (E/V vs Hg/HgO) for NiOOH@GDL-B.

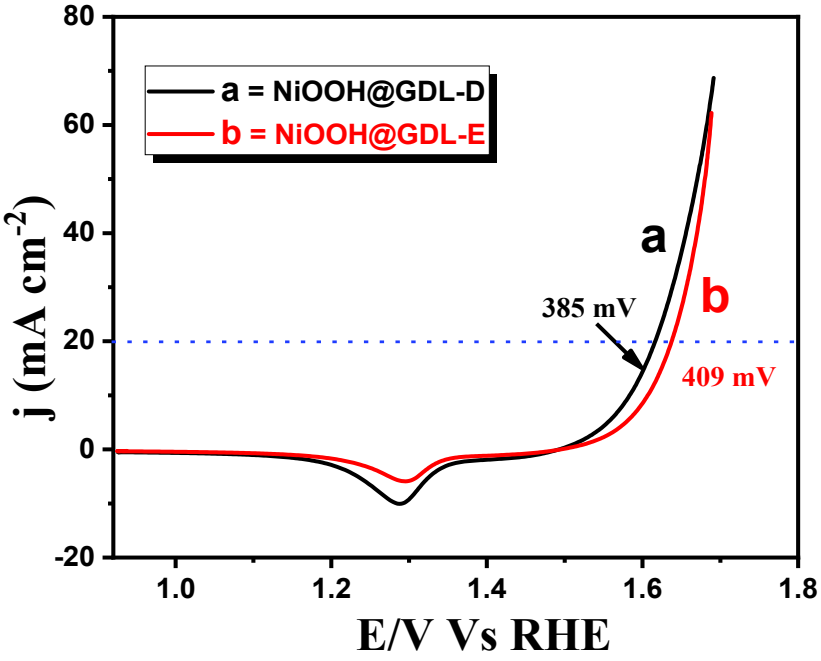

Figure S6. Backward CV curve for the low concentrated catalyst NiOOH@GDL-D (a) and NiOOH@GDL-E (b) for comparison study.

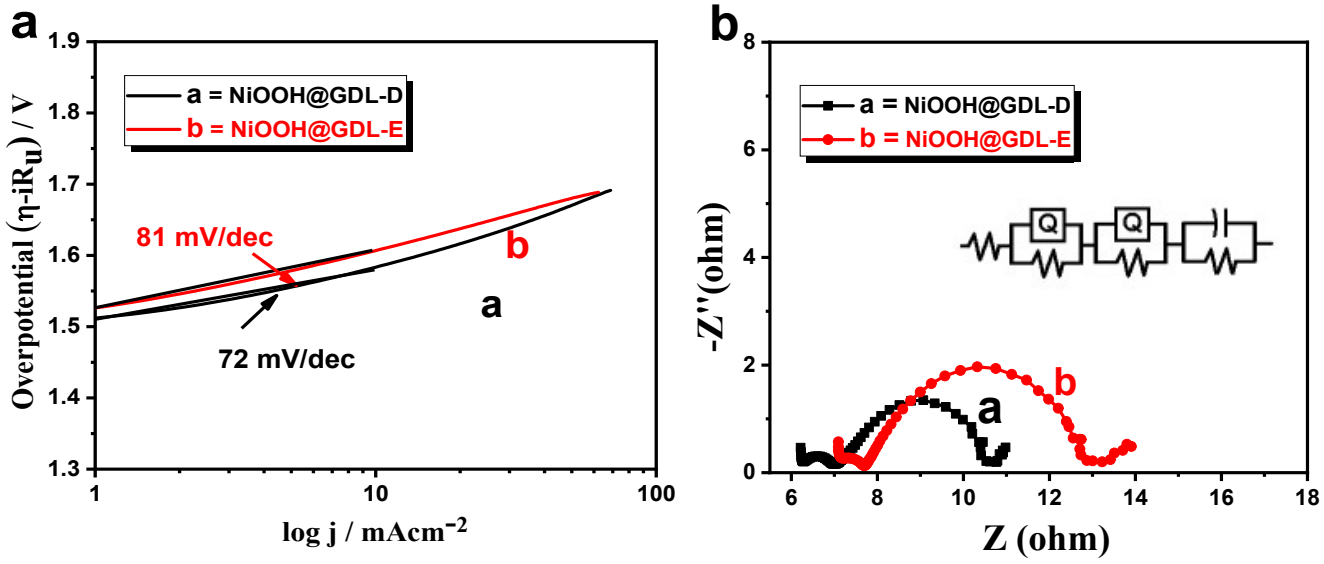

Figure S7. (a) Tafel slope and (b) EIS analysis of low concentrated catalyst NiOOH@GDL-D and NiOOH@GDL-E for comparison study.

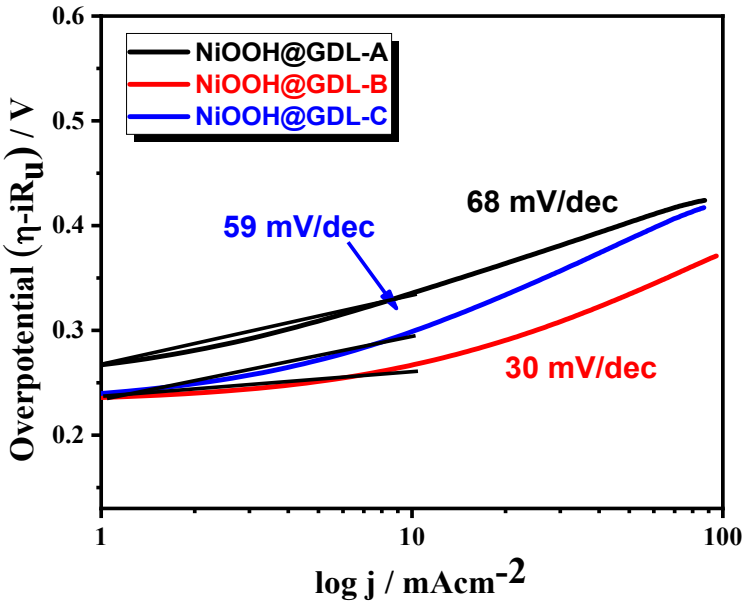

Figure S8. Post Tafel slope analysis for various Conc. NiOOH@GDL performed after cycling study.

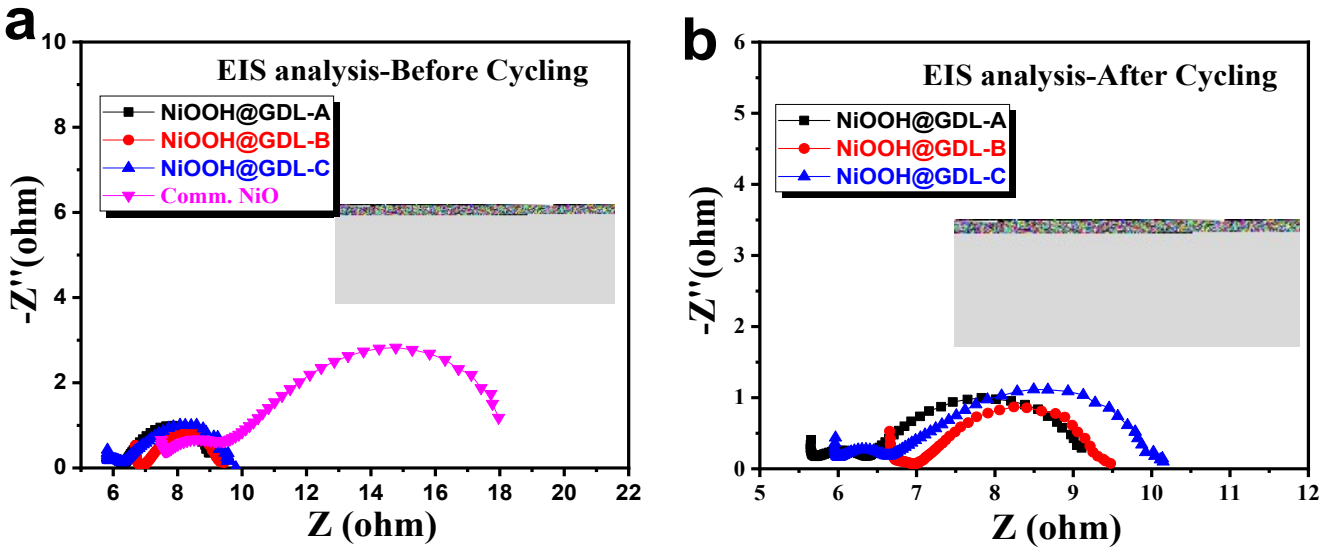

Figure S9. Electrochemical impedance analysis of (a) before cycling NiOOH catalysts and (b) after cycling various NiOOH catalyst at 444 mV overpotential.

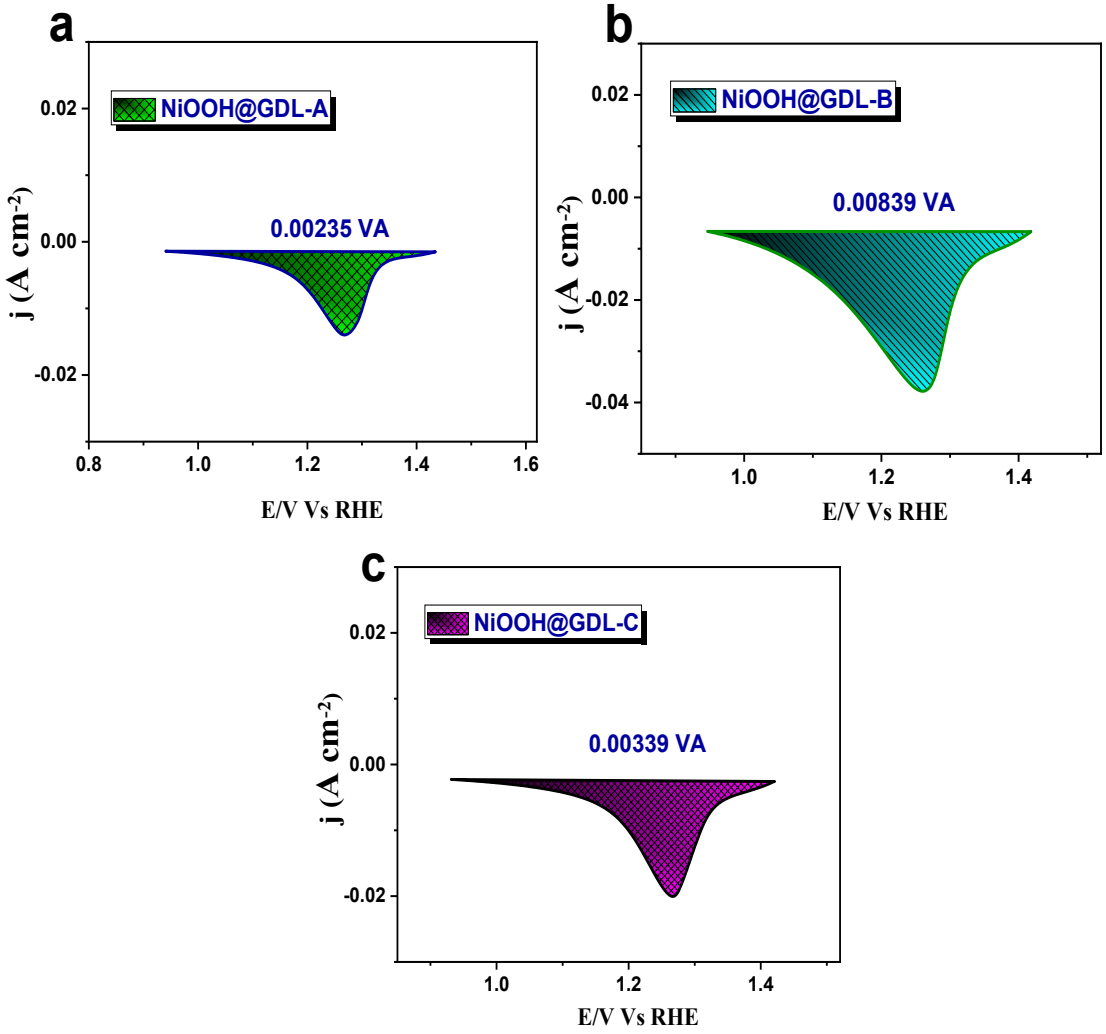

Figure S10. (a-c) After cycling, ECSA calculated from the redox curve from the CV cycle shows the surface area value for all the three catalysts.

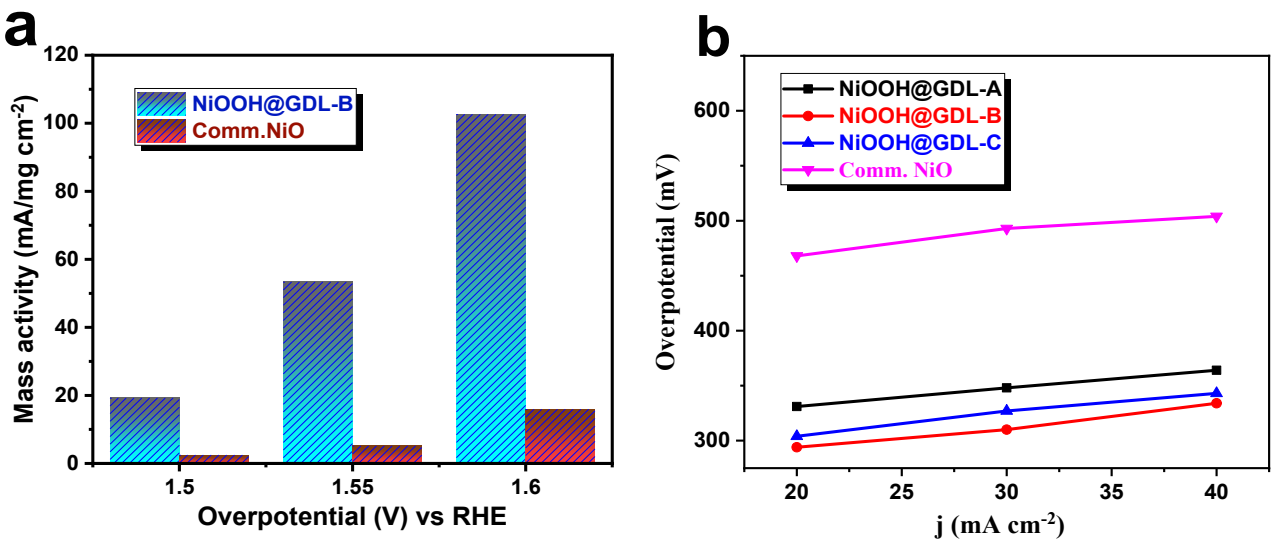

Figure S11. (a) Mass activity calculated at different potential value and (b) the current density vs overpotential plot for all three catalyst compared with comm. NiO.

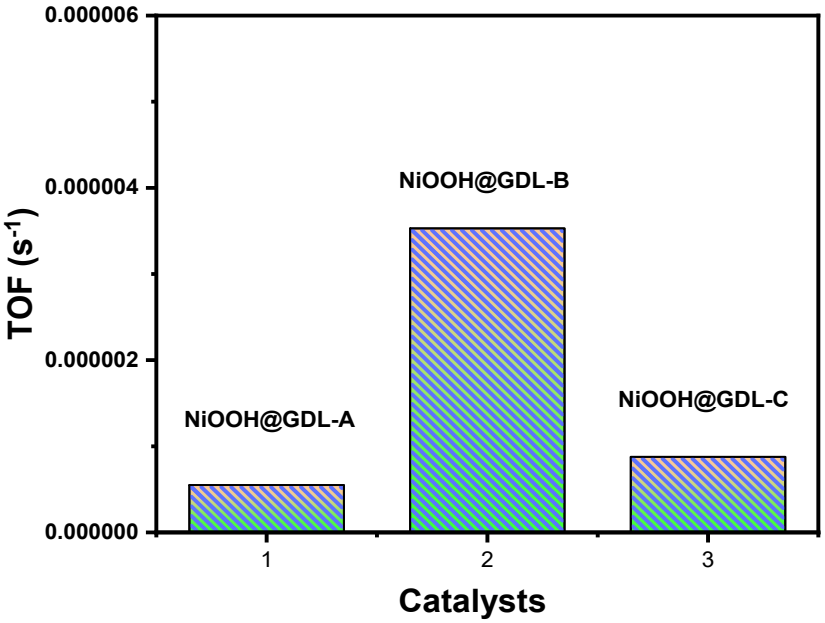

Figure S12. Turnover frequency (TOF) calculated for all the three NiOOH@GDL catalysts at 300 mV overpotential.

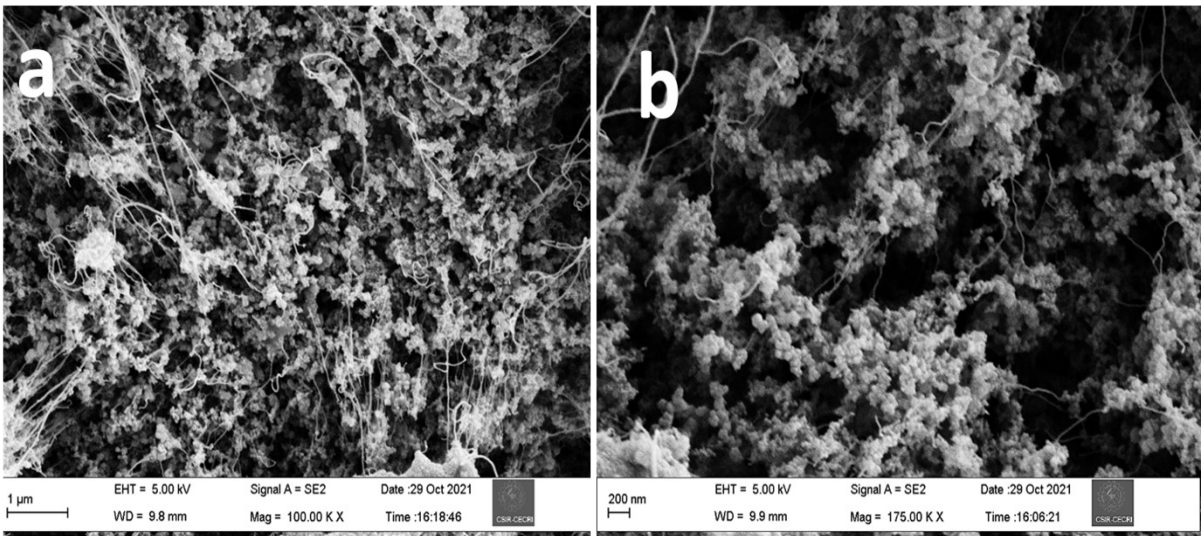

Figure S13. (a, b) Low and high magnified post morphological analysis with FE-SEM image of NiOOH@GDL performed after cycling study.

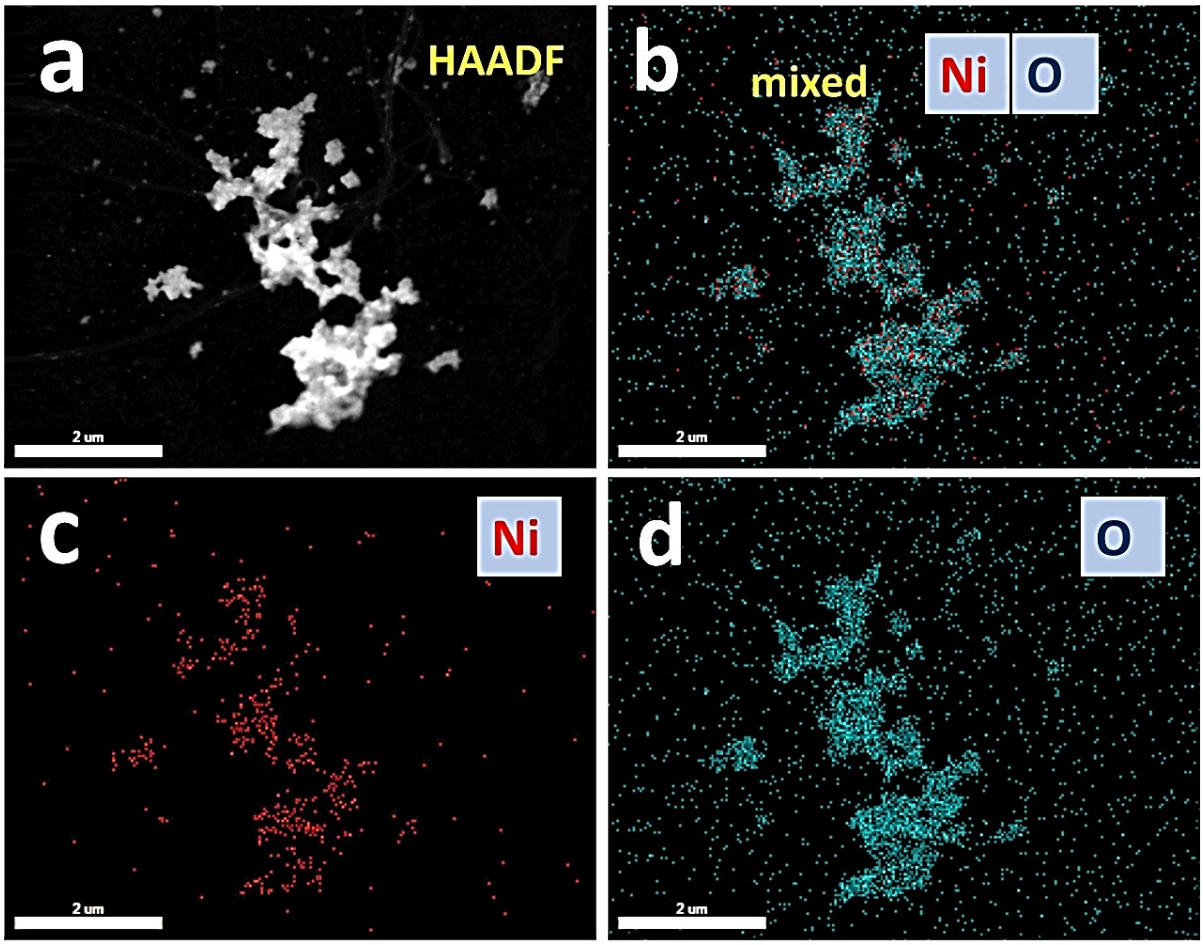

Figure S14. (a-d) are the post-HAADF colour mapping of NiOOH@GDL performed after cycling confirming the presence of Ni and O.

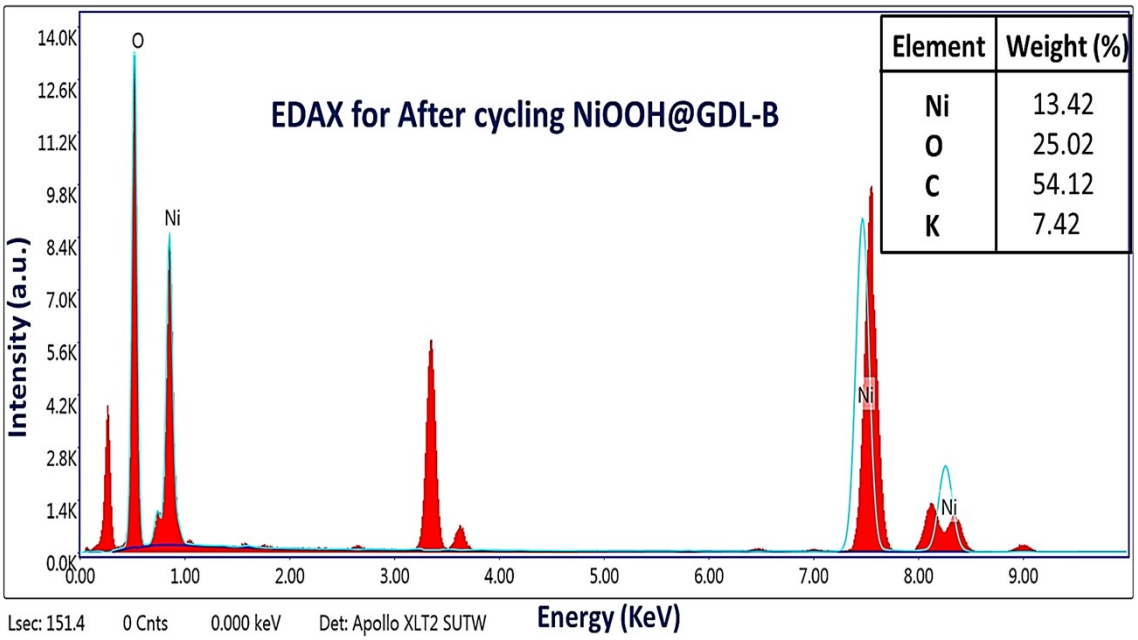

Figure S15. Post EDAX spectra for NiOOH@GDL performed after cycling study.

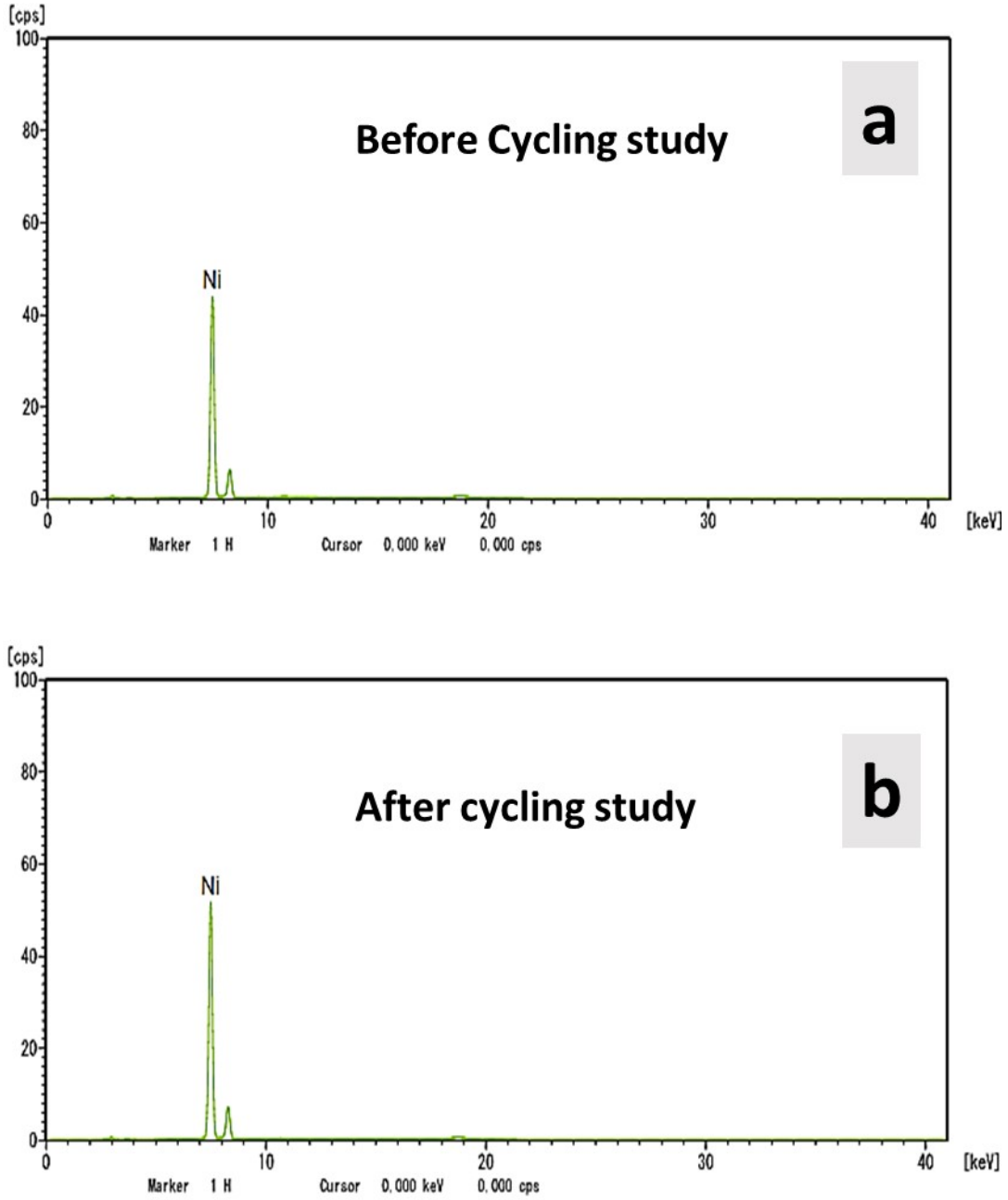

Figure S16. XRF spectrum of NiOOH@GDL-B performed before (a) and after (b) cycling study.

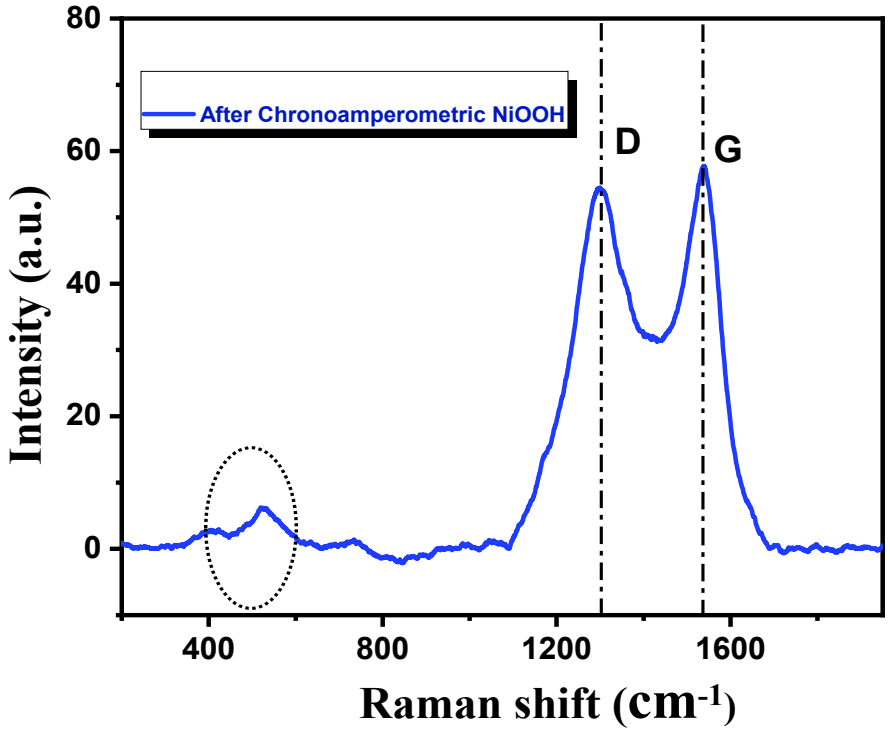

Figure S17. Raman spectra of after chronoamperometric NiOOH@GDL-B.

Table S1. Optimization information of stable NiOOH modified over GDL.

S. No	Parental Concentration of $Ni(OCOCH_3)_2.4H_2O$ Solution (M) in 10 mL DI water	Amount of $Ni(OCOCH_3)_2.4H_2O$ (in gms)	Volume of $Ni(OCOCH_3)_2.4H_2O$ Solution taken from the parental solution (μL)	Volume of DI H_2O (mL) used to prepare the parental $Ni(OCOCH_3)_2.4H_2O$ solution	Solution state	Name of the catalyst
1.	0.3	0.746	34.5	10	Dissolved	NiOOH@GDL-A
2.	0.5	1.244	34.5	10	Dissolved	NiOOH@GDL-B
3.	0.7	1.741	34.5	10	Dissolved	NiOOH@GDL-C
4.	0.05	0.124	34.5	10	Dissolved	NiOOH@GDL-D
5.	0.1	0.248	34.5	10	Dissolved	NiOOH@GDL-E
6.	1	2.488	-	10	Not dissolved (not used in EC studies)	NiOOH@GDL-F
7.	1.5	3.732	-	10	Not dissolved (not used in EC studies)	NiOOH@GDL-G

Table S2. Comparison of OER performance of NiOOH@GDL-B catalyst with other Ni-oxide catalyst in terms of methodology, overpotential, Tafel slope and binder.

Catalysts	Synthesis methods	Medium	Overpotential (mV)	Tafel (mV/dec)	Binder	substrate	Ref. no
Au/NiO_x RT	Sputtering	0.1 M KOH	390 @10 mA cm^{-2}	35	-	Gold disc	1
3D-NiO	Hydrother-mal	1 M KOH	370 @50 mA cm^{-2}	-	Nafion	Glassy carbon	2
2h-Ni/NiO SPE	Solution combustion	1 M KOH	231@10 mA cm^{-2}	108	-	Screen printed graphite	3
NiO NFB	Calcination	1 M KOH	322@10 mA cm^{-2}	78.8	Nafion	Ni foam	4
NiO	Dealloying	1 M KOH	356@20 mA cm^{-2}	76.73	PTFE	Ni foam	5
Ni0-200nm	Chemical bath deposition	1 M KOH	345@10 mA cm^{-2}	48	-	Quartz/Ti/Au	6
NiO nanosheets	Chemical growth	1 M KOH	340@20 mA cm^{-2}	97	-	Ni foam	7
0.5 wt% Pt/NiO	Nano-casting	1 M KOH	358@10 mA cm^{-2}	33	-		8
Ni-$Ni(OH)_2$	Electrodep-osition	1 M KOH	290@10 mA cm^{-2}	120	-	Cu foil	9
Ni_2.2Fe($OH)_x$	Electrodep-osition	1 M KOH	298@100 mA cm^{-2}	64.3	-	Cu foam	10
Holey $Ni(OH)_2$	Etching	1 M KOH	335@10 mA cm^{-2}	65	Nafion	Glassy carbon	11
α- $Ni(OH)_2$	Hydrother-mal	0.1 M KOH	331@10 mA cm^{-2}	42	Nafion	Glassy carbon	12
NiOOH@ GDL-B	***In-situ* formation**	**1 M KOH**	**294@20 mA cm^{-2}**	**30**	**-**	**Carbon cloth**	**This work**

Table S3. Comparison of OER performance of NiOOH@GDL-B catalyst with other transition metal based catalyst in terms of methodology, overpotential, Tafel slope and binder.

Catalysts	Synthesis methods	Medium	Overpotential	Tafel (mV/dec)	Binder	Substrate	Ref. no.
NiAl-LDH/NF	Hydrothermal	1 M KOH	314@10mA cm^{-2}	93	-	Ni foam	13
NiFe-LDH/CNT	Solvothermal	1 M KOH	250@10 mA cm^{-2}	31	-	Glassy carbon	14
Ni_3Se_4	Wet chemical technique	1 M KOH	370@10 mA cm^{-2}	30	Nafion	Carbon cloth	15
Co-doped $NiSe_2$	Electrodeposition	1 M KOH	320@100 mA cm^{-2}	42	No binder	Ti plate	16
$Ni_{0.88}Co_{1.22}Se$	Wet chemical technique	1 M KOH	340@10 mA cm^{-2}	78	Nafion	FTO	17
Ni_3Se_2	Electrodep-osition	0.3 M KOH	310@10 mA cm^{-2}	97.1	No binder	Au-coated glass substrate	18
Ni-Co-Se/CFP	Solvother-mal	1 M KOH	300@10 mA cm^{-2}	87	No binder	carbon fiber paper CFP	19
NiCo-LDH nanoplates	Hydrother-mal	1 M KOH	307@10 mA cm^{-2}	68	Nafion	Carbon fiber paper	20
Ni-Fe-MoO_4-LDH	Solvother-mal	0.1 M KOH	491@10 mA cm^{-2}	23	-	Glassy carbon	21

NiVP@NiFeV-LDH/NF	Hydrother-mal	1 M KOH	317@100 mA cm^{-2}	83	-	Ni foam	22
NiCu-MOFNs/NF	Hydrother-mal	1 M KOH	309@100 mA cm^{-2}	107.2	-	Ni foam	23
NiOOH @GDL-B	***In-situ* transfor mation**	**1 M KOH**	**294@20 mA cm^{-2}**	**30**	**-**	**Carbon cloth**	**This work**

References

1 H. Radinger, P. Connor, S. Tengeler, R. W. Stark, W. Jaegermann and B. Kaiser, *Chem. Mater.*, 2021, **33**, 8259–8266.

2 D. Takimoto, S. Hideshima and W. Sugimoto, *ACS Appl. Nano Mater.*, 2021, **4**, 8059–8065.

3 N. Srinivasa, J. P. Hughes, P. S. Adarakatti, C. Manjunatha, S. J. Rowley-Neale, S. Ashoka and C. E. Banks, *RSC Adv.*, 2021, **11**, 14654–14664.

4 V. D. Silva, T. A. Simões, J. P. F. Grilo, E. S. Medeiros and D. A. Macedo, *J. Mater. Sci.*, 2020, **55**, 6648–6659.

5 X. Ren, Y. Zhai, Q. Zhou, J. Yan and S. Liu, *J. Energy Chem.*, 2020, **50**, 125–134.

6 S. Cosentino, M. Urso, G. Torrisi, S. Battiato, F. Priolo, A. Terrasi and S. Mirabella, *Mater. Adv.*, 2020, **1**, 1971–1979.

7 D. Jia, H. Gao, L. Xing, X. Chen, W. Dong, X. Huang and G. Wang, *Inorg. Chem.*, 2019, **58**, 6758–6764.

8 C. Lin, Y. Zhao, H. Zhang, S. Xie, Y. F. Li, X. Li, Z. Jiang and Z. P. Liu, *Chem. Sci.*, 2018, **9**, 6803–6812.

9 M. Y. Gao, C. B. Sun, H. Lei, J. R. Zeng and Q. B. Zhang, *Nanoscale*, 2018, **10**, 17546–17551.

10 T. Zhou, Z. Cao, P. Zhang, H. Ma, Z. Gao, H. Wang, Y. Lu, J. He and Y. Zhao, *Sci. Rep.*, 2017, **7**, 46154.

11 X. Kong, C. Zhang, S. Y. Hwang, Q. Chen and Z. Peng, *Small*, 2017, **13**, 1700334.

12 M. Gao, W. Sheng, Z. Zhuang, Q. Fang, S. Gu, J. Jiang and Y. Yan, *J. Am. Chem. Soc.*, 2014, **136**, 7077–7084.

13 L. Feng, Y. Du, J. Huang, L. Cao, L. Feng, Y. Feng, Q. Liu, D. Yang and K. Kajiyoshi, *Sustain. Energy Fuels*, 2020, **4**, 2850–2858.

14 M. Gong, Y. Li, H. Wang, Y. Liang, J. Z. Wu, J. Zhou, J. Wang, T. Regier, F. Wei and H. Dai, *J. Am. Chem. Soc.*, 2013, **135**, 8452–8455.

15 S. Anantharaj, E. Subhashini, K. C. Swaathini, T. S. Amarnath, S. Chatterjee, K. Karthick and S. Kundu, *Appl. Surf. Sci.*, 2019, **487**, 1152–1158.

16 T. Liu, A. M. Asiri and X. Sun, *Nanoscale*, 2016, **8**, 3911–3915.

17 D. V. Shinde, L. De Trizio, Z. Dang, M. Prato, R. Gaspari and L. Manna, *Chem. Mater.*, 2017, **29**, 7032–7041.

18 A. T. Swesi, J. Masud and M. Nath, *Energy Environ. Sci.*, 2016, **9**, 1771–1782.

19 K. Ao, J. Dong, C. Fan, D. Wang, Y. Cai, D. Li, F. Huang and Q. Wei, *ACS Sustain. Chem. Eng.*, 2018, **6**, 10952–10959.

20 C. Yu, Z. Liu, X. Han, H. Huang, C. Zhao, J. Yang and J. Qiu, *Carbon N. Y.*, 2016, **110**, 1–7.

21 K. Nejati, S. Davari, A. Akbari, K. Asadpour-Zeynali and Z. Rezvani, *Int. J. Hydrogen Energy*, 2019, **44**, 14842–14852.

22 X. Zou, X. Wei, W. Bao, J. Zhang, P. Jiang and T. Ai, *Int. J. Hydrogen Energy*, 2021, **46**, 32385–32393.

23 X. Zheng, X. Song, X. Wang, Z. Zhang, Z. Sun and Y. Guo, *New J. Chem.*, 2018, **42**, 8346–8350.